

Combined Quantum Mechanical and Molecular Mechanics Studies of the Electron-Transfer Reactions Involving Carbon Tetrachloride in Solution

Marat Valiev* and Eric J. Bylaska

William R. Wiley Environmental Molecular Sciences Laboratory, Pacific Northwest National Laboratory, P.O. Box 999, Richland, Washington, 99352

Michel Dupuis

Fundamental Sciences Division, Pacific Northwest National Laboratory, P.O. Box 999, Richland, Washington 99352

Paul G. Tratnyek

OGI School of Science & Engineering, Oregon Health & Science University, 20000 Northwest Walker Road, Beaverton, Oregon 97006-8921

Received: October 30, 2007; In Final Form: December 25, 2007

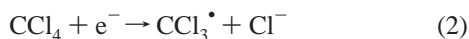
The reductive dechlorination of carbon tetrachloride, CCl₄, by a concerted electron transfer-bond breaking mechanism was studied using combined high level quantum mechanical and molecular mechanics (QM/MM) approach. The free energy activation barriers for the first electron-transfer step were determined from the dissociation profiles of CCl₄ and [•]CCl₄⁻ complexes in aqueous phase using hybrid-free energy QM/MM methodologies. Both density functional and coupled cluster perturbative triples (CCSD(T)) versions of QM/MM methods were investigated. The impact of the implicit solvent description based on continuum (COSMO) solvent models was also analyzed. QM/MM calculations at the CCSD(T)/aug-cc-pVDZ/SPCE level of theory predict that the activation barriers vary from 0.7 to 35.2 kcal/mol for -2.32 and 0.93 V reduction potentials respectively. Good agreement with experimental data for oxide-free iron electrodes (-0.6 to -1.2 V reduction potentials) is observed indicating that the measured activation barriers are consistent with the concerted electron transfer-bond-breaking mechanism.

I. Introduction

It is well documented that mineral surfaces,¹⁻⁴ sulfides,² electron carriers such as quinones⁵⁻⁸ and iron(II) porphyrins,⁵⁻⁸ and microbes^{9,10} facilitate the degradation of carbon tetrachloride in subsurface environments. The majority of these processes are known to transform carbon tetrachloride by the following 2e⁻ redox reaction:¹¹



This dechlorination process is assumed to occur in two sequential electron transfers (ET) steps: the first ET step, which is thought to be rate-limiting,¹² is a dissociative electron attachment (DEA) reaction leading to the formation of a trichloromethyl radical and a chloride ion.



The CCl₃[•] + Cl⁻ dissociation channel is favored over CCl₃⁻ + Cl both on the basis of experimental electron affinities (2.173 eV for CCl₃¹³ and 3.61 eV for Cl¹⁴) and ab initio calculations.¹⁵ The second ET step for the hydrogenolysis reaction allows the newly formed radical to bind to a proton and form a neutral compound



The rates of degradation of these species and the factors controlling reduction processes and rates are not well understood. Their full characterization requires a detailed description of the (rate determining) mechanisms. Even though quantitative structure–activity relationships for chemical reductions of organic contaminants have proven valuable in predicting reaction rates,¹⁶ the implied correlations often appear to be counter intuitive. For example, the overall redox reactions for the chlorinated methanes are all highly exothermic, however the rates of dechlorination are significantly different with each successive dechlorination step proceeding significantly slower.^{16,17}

Detailed molecular information about these processes can be in principle provided by computational modeling based on accurate ab initio methodologies. Several groups have been interested in applying such methods to study the environmental degradation of chlorinated organic compounds.^{15,18–36} Electronic structure calculations for the reduction of chlorinated methanes have been previously reported^{15,37} and recently activation energies for the reduction of CCl₄ have also been calculated.³⁶ There are several outstanding issues, however, that remain to be addressed to ensure the reliability of such applications. On one hand, a sufficiently high level of ab initio theory is needed for accurate description of electronic correlation effects; on the other hand, the presence of the aqueous environment and its finite temperature fluctuations must be properly accounted for.

* To whom correspondence should be addressed.

Phenomenological continuum solvation models, such as COSMO³⁸ and PCM³⁹ have shown to be reliable in predicting equilibrium solvation energies for many environmental degradation reactions. However, less is known about their reliability for modeling reactions pathways and transition states. In these cases, explicit atomistic description of the aqueous environment may be required.

A particular efficient methodology that enables explicit treatment of the environment can be found in the combined quantum mechanical molecular mechanics (QM/MM) approach.^{40,41} This methodology breaks the system into a quantum mechanical (QM) region treated at a quantum mechanical level of theory surrounded by a molecular mechanics (MM) region treated at the classical molecular mechanics level of theory. This approach greatly expedites total energy/gradient calculations, taking advantage of the intrinsic solvent–solute separation in the system. Still, until recently applications of the QM/MM methodology with high level QM descriptions were quite limited. The main challenge was lack of efficient and practical schemes for the QM/MM calculations of free energy, the quantity essential for the characterization of reaction processes in aqueous solution. With recent advances in parallel hardware/software and the development of new free energy methods, this situation has been rapidly changing. Recently, we reported⁴² the implementation of a new QM/MM protocol that allows free energy calculations even when using high levels of ab initio theories. This is the approach that we take in this work. The accuracy and reliability of our quantum-mechanical description is established by utilizing different levels of electronic structure theory from density functional theory (DFT) to high level CCSD(T)^{43,44} methods. As explained in Section IIC, the dissociation pathway is obtained based on the efficient optimization procedure of the entire solute–solvent complex supplemented by dynamical equilibration. The computed reaction barriers fully account for dynamical effects of the solvent by means of multilevel⁴² free energy cycles where thermodynamical averages are performed over many solvent configuration accessible in finite temperature conditions. The QM/MM free energy calculations are also compared against COSMO³⁸ continuum solvation description, which offers further insight into applicability of implicit solvent models. Computational techniques presented in our work are general in nature and readily applicable to thermal reactions. Their applications to the degradation of carbon tetrachloride demonstrates how they can be applied to the more computationally challenging electron-driven processes in aqueous medium.

II. Computational Approach

A. Activation Barriers. Following the strategy suggested by Saveant and co-workers,^{29,45,46} the activation energy (E_{act}) of the concerted ET reaction (corresponding to a dissociative electron attachment), eq 2, can be estimated by finding the crossing point between the dissociation potential energy curves for the neutral and the anion CCl_4 species as a function of the C–Cl bond length^{29,31,45} (see Figure 1). The relative positions of the two dissociation curves and subsequently the activation energy depend on the redox potential (W_0) of the reducing agent that provides the electron for the DEA of CCl_4 . As the strength of reducing agent increases (W_0 is more negative), the anion dissociation curve moves down and the height of the activation barrier decreases. Conversely, as the strength of reducing agent decreases (W_0 is less negative), the activation barrier increases. In the above description, we omitted the zero-point and entropic changes associated with the other vibrational modes besides

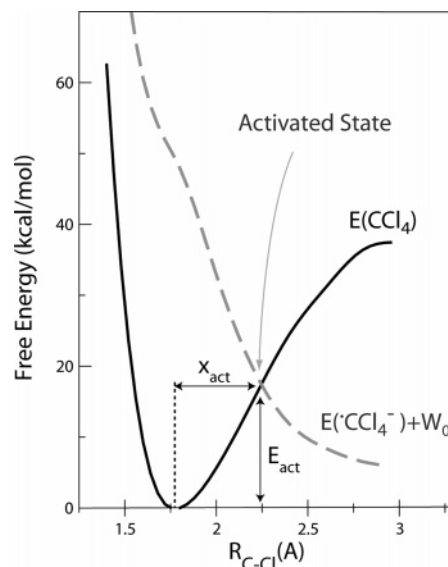


Figure 1. Illustration of curve crossing in the dissociative electron-transfer model. Solid and dashed curves refer to the dissociation of the neutral and anion CCl_4 species, respectively. W is the work function of the reducing agent.

C–Cl stretching. In the range of C–Cl distances around the crossing point, we make the assumption that changes to the other vibrational modes (orthogonal to the C–Cl reaction coordinate) are likely to be small and that the primary zero-point and entropic changes during the course of the reaction will be associated with C–Cl stretch.

B. Gas-Phase Calculations. Activation barriers in the gas phase were calculated using both DFT and CCSD(T) levels of theory. Calculations were performed at the double- ζ quality basis sets, as those were demonstrated to provide a reasonable description of chlorinated hydrocarbon systems.^{15,18} Similar to prior calculations,³⁶ DFT calculations were based on the B3LYP^{47,48} exchange correlation functional with 6-31+G* basis set.⁴⁹ The CCSD(T) calculations were carried out with the aug-cc-pVDZ⁵⁰ basis set. The dissociation pathway was constructed using a series of constrained geometry optimizations of neutral CCl_4 , with $R_{\text{C-Cl}}$ distances ranging from 1.4 to 3.6 Å by increments of 0.1 Å. These optimized DFT geometries were then used for the CCSD(T) calculations. The NWChem program suite was used to perform these calculations.⁵¹

C. QM/MM Calculations. QM/MM Description. In aqueous solution, the activation barriers were determined using the QM/MM approach. In this method, the total energy of the system is given by the sum of the quantum (E_{qm}) and classical energies (E_{mm})

$$E = E_{\text{qm}}[\mathbf{r}, \mathbf{R}; \psi] + E_{\text{mm}}[\mathbf{R}, \mathbf{r}] \quad (5)$$

where \mathbf{r} , \mathbf{R} represent the coordinates of QM and MM regions, respectively, and ψ denotes the ground-state electronic wavefunction of the QM region. The QM energy can be conveniently separated into internal and external contributions⁴²

$$E_{\text{qm}}[\mathbf{r}, \mathbf{R}; \psi] = E_{\text{qm}}^{\text{int}}[\mathbf{r}; \psi] + E_{\text{qm}}^{\text{ext}}[\mathbf{r}, \mathbf{R}; \rho] \quad (6)$$

The internal part $E_{\text{qm}}^{\text{int}}[\mathbf{r}; \psi]$ is the gas-phase energy expression. The external part $E_{\text{qm}}^{\text{ext}}[\mathbf{r}, \mathbf{R}; \rho]$ contains the electrostatic interactions of the classical charges (Z_i) of the MM region with the electron density (ρ)

$$E_{\text{qm}}^{\text{ext}}[\mathbf{r}, \mathbf{R}; \rho] = \sum_I \int \frac{Z_I \rho(\mathbf{r}')}{|\mathbf{R}_I - \mathbf{r}'|} d\mathbf{r}' \quad (7)$$

Finally the last term in eq 5, the classical energy (E_{mm}), contains all the classical interactions in the MM system, involving both the solvent Coulomb and van der Waals energies and the solute–solvent van der Waals interactions.

Unlike gas phase, the dissociation process in the aqueous environment can no longer be described in the terms of total energy but rather requires free-energy description to capture the entropic effects associated with the solvent fluctuations at finite temperature. With the assumption that solvent MM region is able to rapidly equilibrate with different solute configurations during dissociation, the solvent degrees of freedom can be averaged out⁵² leading to the definition of potential of mean force (PMF)

$$W(\mathbf{r}, \beta) = -\frac{1}{\beta} \ln \int e^{-\beta E(\mathbf{r}, \mathbf{R}; \psi)} d\mathbf{R} \quad (8)$$

where $\beta = 1/kT$. The PMF difference between the two points A and B on the dissociation pathway characterized by \mathbf{r}_A and \mathbf{r}_B solute configurations of the solute CCl_4 region is given by

$$\Delta W_{\text{AB}} = -\frac{1}{\beta} \ln \langle e^{-\beta(E(\mathbf{r}_B, \mathbf{R}; \psi_B) - E(\mathbf{r}_A, \mathbf{R}; \psi_A))} \rangle_{\mathbf{r}_A} \quad (9)$$

where the angular brackets denote a statistical averaging over solvent configurations with fixed solute geometry

$$\langle \dots \rangle_{\mathbf{r}} = \frac{\int \dots e^{-\beta E(\mathbf{r}, \mathbf{R}; \psi)} d\mathbf{R}}{\int e^{-\beta E(\mathbf{r}, \mathbf{R}; \psi)} d\mathbf{R}} \quad (10)$$

System Setup. Our system contained CCl_4 molecule embedded into a 30 Å cubic solvent box containing 890 water molecules. Periodic boundary conditions were used. The QM region consisted of CCl_4 and the MM region included all the water molecules. The QM region was treated quantum mechanically using either the DFT level of theory with the B3LYP^{47,48} exchange correlation functional or the coupled cluster theory (CCSD(T))⁴⁴ level of theory. The 6-31+G* basis set⁴⁹ was used for the DFT calculations and the aug-cc-pVDZ⁵⁰ basis set was used for the CCSD(T) calculations. The MM water molecules were described using classical SPC/E model.⁵³ The van der Waals parameters for the quantum region were taken from standard Amber force field definitions.⁵⁴ Cutoff radius for classical interactions was set at 15 Å.

Dissociation Pathway The dissociation pathway was constructed by stretching one of the C–Cl bonds in the neutral state of CCl_4 in 0.2 Å increments with initial and final distance of 1.4 and 3.6 Å, respectively. Keeping the two atoms of the dissociating bond fixed, the rest of the system, including the solvent molecules, was optimized at each point on the pathway. As in our previous work⁴² the optimization procedure relied on the zero-temperature approximation of the derivatives of $W(\mathbf{r}, \beta)$

$$\lim_{\beta \rightarrow \infty} \partial_{\mathbf{r}} W(\mathbf{r}, \beta) = \partial_{\mathbf{r}} E(\mathbf{r}, \mathbf{R}^*; \psi) \quad (11)$$

where \mathbf{R}^* is the solvent configuration that minimizes E for a given \mathbf{r} and ψ . To facilitate determination of the optimized solvent configuration \mathbf{R}^* , an effective classical charge representation^{42,55} (ESP) of the solute electron density was used to calculate the solute–solvent interactions

$$\sum_I \int \frac{Z_I \rho(\mathbf{r}')}{|\mathbf{R}_I - \mathbf{r}'|} d\mathbf{r}' = \sum_{i,I} \frac{Z_i Q_i}{|\mathbf{R}_I - \mathbf{r}'|} \equiv E_{\text{esp}}(\mathbf{r}, \mathbf{R}; Q) \quad (12)$$

Here, effective solute charges (Q_i) are chosen to fit the correct electrostatic potential outside the solute region. To ensure a minimum solvent structure, the optimization process was also supplemented by dynamical equilibration of the solvent utilizing effective classical charge representation (see eq 12).

PMF Calculations. Our PMF calculations were based on the strategy described in our previous work.⁴² To avoid extreme computational expense involved in direct evaluation of eq 9, we used a multilevel thermodynamic cycle based on several QM/MM representations:⁴² the CCSD(T)/MM, DFT/MM, and ESP/MM. CCSD(T)/MM and DFT/MM representations were obtained by replacing the internal energy term in eq 6 by the appropriate CCSD(T) and DFT expressions, respectively. The ESP/MM representation was obtained by simply replacing E_{qm} in eq 6 by the effective charge energy E_{esp} (see eq 12). The total free energy difference ΔW_{AB} was then calculated as a sum of three contributions (see Figure 2)

$$\Delta W_{\text{AB}} = \Delta W_{\text{AB}}^{\text{cc} \rightarrow \text{dft}} + \Delta W_{\text{AB}}^{\text{dft} \rightarrow \text{esp}} + \Delta W_{\text{AB}}^{\text{esp}} \quad (13)$$

The first two terms represent the free energy differences associated with changing the description of the fixed solute region from the CCSD(T) to the DFT representations and from the DFT to the classical ESP representations.

$$\begin{aligned} W^{\text{cc} \rightarrow \text{dft}} &= \Delta W_{\text{AA}}^{\text{cc} \rightarrow \text{dft}} - \Delta W_{\text{BB}}^{\text{cc} \rightarrow \text{dft}} \\ W^{\text{dft} \rightarrow \text{esp}} &= \Delta W_{\text{AA}}^{\text{dft} \rightarrow \text{esp}} - \Delta W_{\text{BB}}^{\text{dft} \rightarrow \text{esp}} \end{aligned} \quad (14)$$

The third term represents the free energy difference associating with changing the solute configuration from (\mathbf{r}_A, Q_A) to (\mathbf{r}_B, Q_B) with the ESP representation of the solute.

Because the changes in representations (CCSD(T) to DFT, DFT to ESP) occur for fixed solute configurations, we can assume that there is little perturbation in the phase space accessible to the solvent. In this case, we can utilize the free energy perturbation theory⁵⁶ to calculate the corresponding free energy differences:

$$\Delta W_{\text{AA}}^{\text{cc} \rightarrow \text{dft}} = -\frac{1}{\beta} \ln \langle e^{-\beta \Delta E_{\text{AA}}^{\text{cc} \rightarrow \text{dft}}} \rangle_{\text{dft/mm}} \quad (15)$$

$$\Delta W_{\text{AA}}^{\text{dft} \rightarrow \text{esp}} = -\frac{1}{\beta} \ln \langle e^{-\beta \Delta E_{\text{AA}}^{\text{dft} \rightarrow \text{esp}}} \rangle_{\text{esp/mm}} \quad (16)$$

where

$$\begin{aligned} \Delta E_{\text{AA}}^{\text{cc} \rightarrow \text{dft}} &= E_{\text{CC}}(\mathbf{r}_A, \mathbf{R}; \psi_A) - E_{\text{dft}}(\mathbf{r}_A, \mathbf{R}; \psi_A) \\ \Delta E_{\text{AA}}^{\text{dft} \rightarrow \text{esp}} &= E_{\text{dft}}(\mathbf{r}_A, \mathbf{R}; \psi_A) - E_{\text{esp}}(\mathbf{r}_A, \mathbf{R}; Q_A) \end{aligned} \quad (17)$$

The calculation of $\Delta W_{\text{AA}}^{\text{cc} \rightarrow \text{dft}}$ can be further simplified⁴² using the fact that DFT (at least in its formal derivation) should generate the exact electron density, which should be fairly well reproduced in the CCSD(T) calculations. Because the electron density is the sole coupling parameter between the solute electronic degrees of freedom and the solvent (see eq 7), we obtain

$$\frac{\delta \Delta E_{\text{AA}}^{\text{cc} \rightarrow \text{dft}}}{\delta \mathbf{R}} \approx 0 \Rightarrow \Delta W_{\text{AA}}^{\text{cc} \rightarrow \text{dft}} \approx \Delta E_{\text{AA}}^{\text{cc} \rightarrow \text{dft}} \quad (18)$$

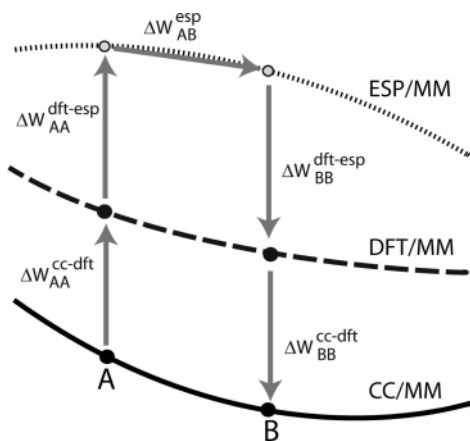


Figure 2. Illustration of multilevel free energy perturbation cycle.

In the calculation of $\Delta W_{AA}^{\text{dft} \rightarrow \text{esp}}$ and $\Delta W_{BB}^{\text{dft} \rightarrow \text{esp}}$, we followed a resampling strategy¹⁶ whereby $\Delta E_{AA}^{\text{dft} \rightarrow \text{esp}}$ is evaluated at certain intervals of configurations along the solvent trajectories generated with the ESP/MM representation. In the present work, we resampled of 100 ps of constant temperature ($T = 298.15$ K) molecular dynamics simulations at intervals of 0.5 ps. In the calculation of $\Delta W_{AA}^{\text{cc} \rightarrow \text{dft}}$ and $\Delta W_{BB}^{\text{cc} \rightarrow \text{dft}}$, we followed eq 18 using the optimized solvent configuration.

The classical $\Delta W_{AB}^{\text{esp}}$ term was evaluated using finite difference thermodynamic perturbation theory

$$\Delta W_{AB}^{\text{esp}} = \int_0^1 \partial_\lambda W^{\text{esp}}(\lambda) d\lambda \quad (19)$$

Here we defined the λ -dependent free energy function as

$$W^{\text{esp}}(\lambda) = -\frac{1}{\beta} \ln \int e^{-\beta E^{\text{esp}}(\mathbf{r}(\lambda), Q(\lambda), \mathbf{R})} d\mathbf{R} \quad (20)$$

based on the linear mapping between A and B configurations:

$$\begin{aligned} \mathbf{r}(\lambda) &= (1 - \lambda)\mathbf{r}_A + \lambda\mathbf{r}_B \\ Q(\lambda) &= (1 - \lambda)Q_A + \lambda Q_B \end{aligned} \quad (21)$$

Using the trapezoidal rule, $\Delta W_{AB}^{\text{esp}}$ was then approximated as

$$\Delta W_{AB}^{\text{esp}} = \frac{1}{2} (\partial_\lambda W^{\text{esp}}(0) + \partial_\lambda W^{\text{esp}}(1)) \quad (22)$$

The derivatives were calculated using the central difference approximation

$$\partial_\lambda W^{\text{esp}}(\lambda) = \frac{\Delta^{+\delta} W^{\text{esp}}(\lambda) - \Delta^{-\delta} W^{\text{esp}}(\lambda)}{2\delta} \quad (23)$$

where

$$\Delta^{\pm\delta} W^{\text{esp}}(\lambda) = -\frac{1}{\beta} \ln \langle e^{-\beta E(\mathbf{r}(\lambda \pm \delta), Q(\lambda \pm \delta), \mathbf{R}) - \beta E(\mathbf{r}(\lambda), Q(\lambda), \mathbf{R})} \rangle_\lambda \quad (24)$$

In the calculation of $\partial_\lambda W^{\text{esp}}(\lambda)$ statistical averaging was performed over 20 ps of molecular dynamics simulations at constant temperature ($T = 298.15$ K) for both end of the interval with $\delta = 0.1$.

Vertical Electron Affinity. The relative position of the two PMF dissociation curves was established by calculating vertical electron affinity ($-\Delta W^{n \rightarrow a}$) (where n and a denote the neutral and anionic states, respectively) at the first point

on the dissociation pathway. As with our PMF calculations, we adopted the following multilevel thermodynamic cycle:

$$\Delta W^{n \rightarrow a} = (\Delta W_{nm}^{\text{cc} \rightarrow \text{dft}} - \Delta W_{aa}^{\text{cc} \rightarrow \text{dft}}) + (\Delta W_{nm}^{\text{dft} \rightarrow \text{esp}} - \Delta W_{aa}^{\text{dft} \rightarrow \text{esp}}) + \Delta W_{na}^{\text{esp}} \quad (25)$$

The first and second terms, related to the changes in QM representations, were already available from the PMF calculations (see discussion above). To evaluate the classical contribution $\Delta W_{na}^{\text{esp}}$, the mutation of the ESP effective charges representing the neutral solute into those representing the anionic solute was performed over ten windows. The final difference was then evaluated using finite difference thermodynamic perturbation theory as described above. To account for long-range electrostatic effects related to the overall change in the charge of the system, $\Delta W_{na}^{\text{esp}}$ was corrected by means of a Born correction term

$$\Delta W_{\text{born}} = \frac{q^2}{2r_c} \left(1 - \frac{1}{\epsilon}\right) \quad (26)$$

with $r_c = 15$ Å, $q = 1$, and $\epsilon = 78.0$.

D. Continuum Calculations. Calculations of activation barriers using the continuum solvation model were based on the self-consistent reaction field theory of Klamt and Schüürmann (COSMO).³⁸ COSMO solvation model was used in prior calculations³⁶ of CCl_4 and is widely available in many computational chemistry codes. The cavity was defined by a set of intersecting atomic spheres with radii suggested by Stefanovich and Truong (H 1.172, C 1.635, and Cl 1.750 Å).⁵⁷ The dielectric constant of water used for all of the solvation calculations was 78.0. Discretization of the atomic spheres involved an iterative refinement of triangles starting from a regular octahedron.³⁸ Three refinement levels yielding 128 points per sphere followed by removal of discretization points from one sphere inside the neighboring spheres were used to define the solute cavity in the solvent.

III. Results and Discussion

A. Gas Phase. Following the protocol described in Section IIB, we calculated the gas-phase dissociation curves of the neutral and anion CCl_4 species at DFT and CCSD(T) levels of theory (see Figure 3). According to our calculations, the neutral CCl_4 molecule undergoes a homolytic dissociation process:



Similar to other calculations,³⁶ we observe a minimum energy structure for neutral CCl_4 at $R_{\text{CCl}} = 1.79$ Å and for anion CCl_4^- molecule around $R_{\text{CCl}} = 2.57$ Å corresponding to a radical-anion long-range complex. No stable anion structure is observed at short R_{CCl} distances. Previous work³⁷ has shown that the activation energy or “crossing point” is highly sensitive to the level of quantum-mechanical treatment, and several authors have suggested that high-level ab initio calculations are needed to obtain accurate results.^{29,30,58–60} Our gas-phase calculations confirm this sensitivity. For the neutral species, the magnitude of the deviation between DFT and CCSD(T) is not uniform and varies depending on the region. While both DFT and CCSD(T) methods (see Figure 3) agree near the minimum point, significant deviations can be observed in the stretched bond region. For the anion curve, the differences between DFT and CCSD(T) are more uniform. The average absolute difference

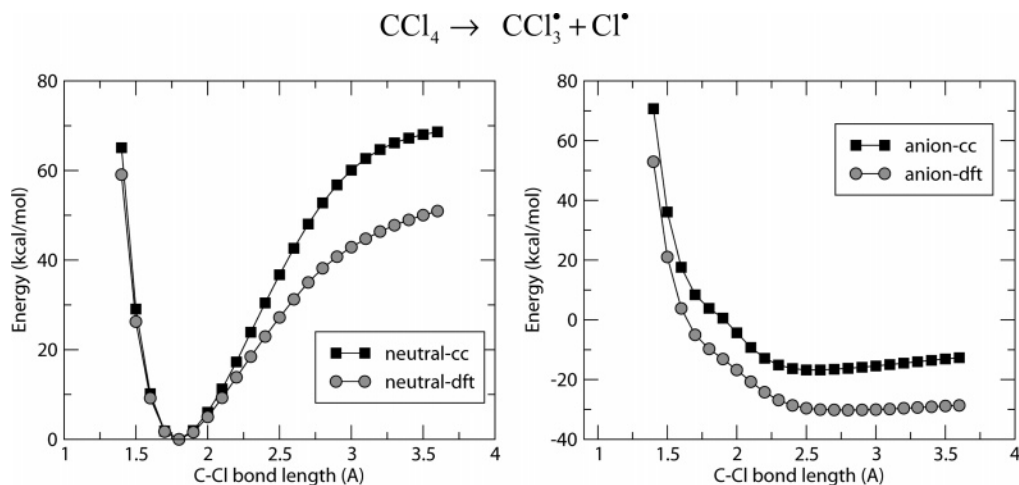


Figure 3. Gas-phase dissociation curves for neutral (left) and anion (right) CCl_4 molecule as a function of dissociating C–Cl bond. Both DFT and CCSD(T) curves are drawn with reference to their respective minima on the neutral dissociation curve.

TABLE 1: Gas Phase Activation Barriers (E_{act}) and Distances (x_{act}) of the Dissociative Electron Attachment Reaction for CCl_4 versus the Ionization Potential of the Reductant (W)

W_0 (kcal/mol)	theory	E_{rxn} (kcal/mol)	E_{act} (kcal/mol)	x_{act} (Å)
−5	DFT	−17.33		
	CCSD(T)		0.80	1.84
0	DFT	−12.33	<0	
	CCSD(T)		1.43	1.87
5	DFT	−7.33		
	CCSD(T)		3.59	1.94
10	DFT	−2.33	0.09	1.81
	CCSD(T)		5.87	2.00
15	DFT	2.67	1.72	1.90
	CCSD(T)		8.42	2.05
20	DFT	7.67	4.13	1.97
	CCSD(T)		10.99	2.10
25	DFT	12.67	6.66	2.04
	CCSD(T)		14.07	2.15
30	DFT	17.67	9.26	2.10
	CCSD(T)		17.19	2.20
35	DFT	22.67	12.08	2.16
	CCSD(T)		20.90	2.25
40	DFT	27.67	15.04	2.23
	CCSD(T)		24.71	2.31

is 14.0 kcal/mol, and the worst case difference is 17.8 kcal/mol at C–Cl distance of 1.4 Å.

Prior calculations of CCl_4 ³⁶ reported significant differences in DFT (11.07 kcal/mol) and MP2 (−15.68 kcal/mol) values for vertical electron affinities of CCl_4 . A similar pattern is observed in our calculations. The vertical electron affinity of CCl_4 is 9.71 kcal/mol at the DFT level and −3.84 kcal/mol at the CCSD(T). The experimental estimate of vertical electron affinity for CCl_4 is predicted to be close to zero (slightly positive).⁶¹ As a result of all these deviations, the DFT estimates of the activation barrier (crossing point) differ significantly from CCSD(T) results (see Table 1). For short activation distances, DFT activation barriers are about 6 kcal/mol below CCSD(T); this difference grows to 9 kcal/mol for long distances.

B. Aqueous Phase. On the basis of QM/MM computational protocol described in Section IIC, we calculated free energy dissociation curves of neutral and anion CCl_4 species in aqueous solution at CCSD(T)/MM level (see Figure 4). Figure 4 also shows individual contributions to the total free energy (see eq 13), which conveniently help the interpretation of the free energy changes during the dissociation process. The W^{esp} component (shown as stars in Figure 4) provides a measure of the changes

in solvation energy during the dissociation. The $W^{\text{esp-dft}}$ component (shown as circles in Figure 4) reflects the contribution from the internal QM energy of the CCl_4 molecule (at the DFT level) corresponding to the energy of the solute by itself, but calculated with the wavefunction polarized by the solvent. Finally $W^{\text{dft-cc}}$ (shown as squares in Figure 4) reflects the “error” in DFT description as compared to the more accurate CCSD(T) description.

Dissociation of neutral CCl_4 molecule is characterized by a large negative shift in W^{esp} for long C–Cl bonds, indicating increased stabilization due to solvation effects. This is consistent with large dipole moment observed in the stretched C–Cl bond regime. DFT/MM calculations show a dipole moment of 15.9 au at $R_{\text{CCl}} = 2.57$ Å, which is significantly larger than the corresponding gas-phase value of 6.0 au. Closer analysis of the molecular orbital structure of neutral dissociated species indicates that unlike gas phase, the dissociation of neutral species in aqueous phase proceeds through the heterolytic channel



leading to the enhanced dipole moment. Consistent with this mechanism, we observe that the internal QM energy of neutral species (see $W^{\text{esp-dft}}$ curve in Figure 4) in aqueous phase shows no saturation in the stretched bond region and has a much higher value compared to its gas-phase counterpart (see Figure 3). In aqueous phase, the energetic costs of the heterolytic state are outweighed by the increased solvation energy (W^{esp}) arising from the larger dipole moment. As indicated by the $W^{\text{dft-cc}}$ free energy contribution (see squares curve in Figure 4), there exists significant differences between DFT and CCSD(T) quantum-mechanical descriptions. Similar to the gas-phase results, the differences are not uniform; they vary with the C–Cl bond length.

The dissociation of anion species is also accompanied by the increase in solvent stabilization energy (see W^{esp} curve in Figure 4). This is consistent with the negative charge redistribution from the larger $^-\text{CCl}_4$ molecule to a more localized charge in the Cl^- ion. The magnitude of this stabilization is less pronounced compared to a neutral case where two ions (CCl_3^+ and Cl^-) are created as a result of dissociation process. The internal QM energy of the anion (see $W^{\text{esp-dft}}$ component in Figure 4) differs from the gas-phase energies, indicating significant polarization effects induced by the aqueous environment. The small magnitude of $W^{\text{dft-cc}}$ (see Figure 4) shows that

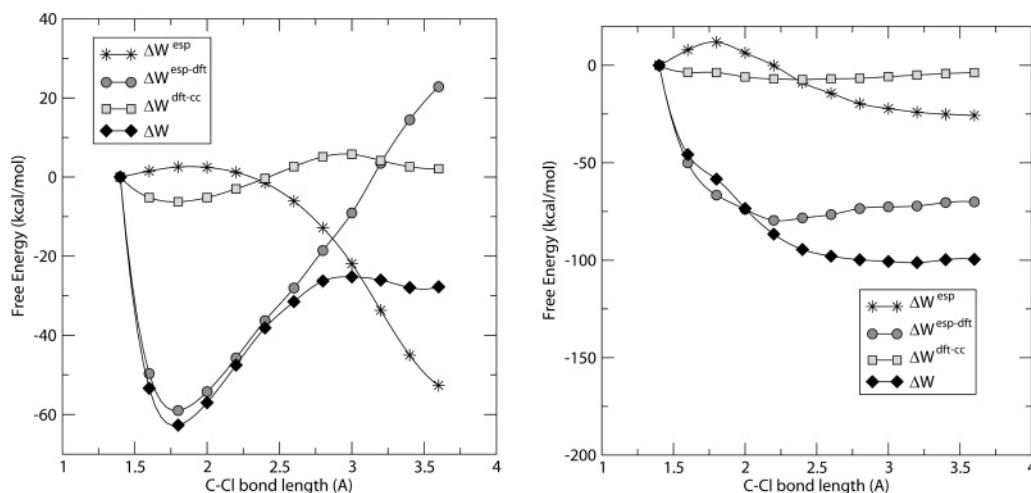


Figure 4. The total PMF (diamonds) for neutral (left) and anion (right) CCl_4 species as a function of dissociating C–Cl bond with individual contributions from CC–DFT (squares), ESP–DFT (circles), and ESP (stars) contributions (see eqs 13 and 14 in text).

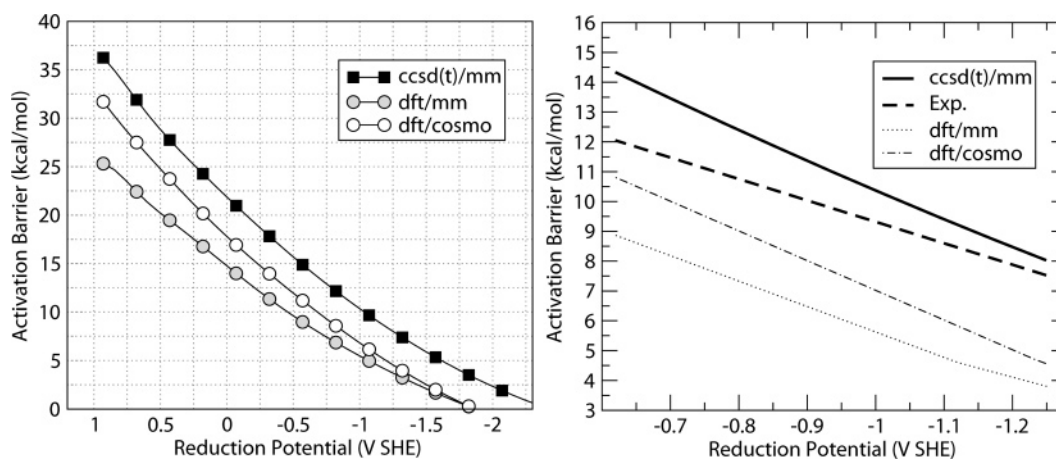


Figure 5. Aqueous phase activation barriers calculated at CCSD(T)/MM, DFT/MM, DFT/COSMO levels of theory (left); comparison between experimental (ref 65) and calculated activation barriers (right).

similar to the gas-phase results the deviations between DFT and CCSD(T) descriptions are more uniform compared to the neutral species.

We find significant deviations between vertical electron affinity (at $R_{\text{CCl}} = 1.4 \text{ \AA}$) calculated with the CCSD(T)/MM (47.17 kcal/mol) and DFT/MM (57.24 kcal/mol) descriptions. In aqueous phase, DFT/MM overestimates the electron affinity by about 10 kcal/mol, compared to 13 kcal/mol error observed in gas phase. The DFT/COSMO calculations show a vertical electron affinity of 54.81 kcal/mol, which is reasonable agreement with DFT/MM results.

The aqueous phase activation barriers calculated at different levels of theory are shown in Figure 5. The reduction potential (work function of the reducing agent) is given with respect to standard hydrogen electrode ($E_{\text{H}}^0 = 98.6 \text{ kcal/mol}$, calculated from $\Delta G_{\text{s}}(\text{H}^+) = -263.98 \text{ kcal/mol}$ ⁶² and $\Delta G_{\text{f}}^0(\text{H}^+_{\text{(g)}}) = 362.58 \text{ kcal/mol}$ ⁶³). In addition, activation barriers (E_{act}), distances (x_{act}), and reaction energies (E_{rxn}) are also reported in Table 2. The calculation of reaction energies was done using reference Gibbs free energies of formation in solution ($\Delta G_{\text{f}}(\text{Cl}^-) = -31.36 \text{ kcal/mol}$, $\Delta G_{\text{f}}(\text{CCl}_4) = -11.25 \text{ kcal/mol}$, $\Delta G_{\text{f}}(\text{CCl}_3^{\bullet}) = 27.01 \text{ kcal/mol}$).^{15,64}

Similar to the gas-phase results, the activation energies were found to be sensitive to the ab initio level of theory. The activation barriers calculated with DFT/MM are on average 4 kcal/mol below CCSD(T)/MM results. As indicated in Figure 5 and Table 2, the activation barriers from DFT/MM and DFT/

COSMO models agree quite well at the low range of reduction potentials ($E_{\text{H}} < -1.5\text{V}$). However, at high reduction potentials the disagreement between DFT/MM and DFT/COSMO models becomes progressively worse (6 kcal/mol difference at $E_{\text{H}} = 0.93 \text{ eV}$). At this range of reduction potentials, the C–Cl bond in the crossing point is nearly cleaved, but it is not long enough to allow complete solvation of dissociating Cl or Cl^- and CCl_3 fragments. Such a situation may be difficult to describe with COSMO parameters tuned for equilibrium situations. At zero reaction energy ($E_{\text{rxn}} = 0$), the activation energy according to DFT/COSMO description is 14.4 kcal/mol compared to 18.8 kcal/mol obtained in the prior work.³⁶

At the CCSD(T)/MM level of theory, the activation barrier varies from a negligible 0.7 kcal/mol for a -2.32 V reduction potential to a modest 35.2 kcal/mol barrier for a 0.93 V reduction potential. As shown in Figure 5, in the range of reduction potentials corresponding to nearly oxide-free iron surfaces⁶⁵ (-0.6 to -1.2V) we find a fairly good agreement between calculated results and experimental data.⁶⁵ Consistent with the trends observed for gas-phase vertical electron affinities, the CCSD(T)/MM description overestimates (~ 0.5 – 2 kcal/mol) and DFT/MM description underestimates ($\sim 3 \text{ kcal/mol}$) the experimental activation energies. At the low range of reduction potentials (-1.2V) that correspond to the activation distances in the equilibrium region, DFT/COSMO description perform similar to DFT/MM. At higher reduction potentials, however, DFT/COSMO exhibits better agreement with experiment (1 kcal/

TABLE 2: Activation Free Energies, Distances, and Reaction Energies of the Aqueous Phase Dissociative Electron Attachment Reaction for CCl₄ versus the Reduction Potential (Experimental Values Are Calculated According to Linear Fit Provided in ref 65)

W_0 (kcal/mol)	W_0 (volts SHE)	theory	E_{rxn} (kcal/mol)	E_{act} (kcal/mol)	x_{act} (Å)	exp E_{act} (kcal/mol)
45	-2.32	DFT/MM	-46.60			
		DFT/COSMO		0.70	1.82	
		CCSD(T)/MM				
55	-1.89	DFT/MM	-36.38			
		DFT/COSMO		3.40	1.92	
		CCSD(T)/MM		2.50	1.91	6.02
65	-1.46	DFT/MM	-27.77	3.01	1.93	
		DFT/COSMO		6.34	2.01	
		CCSD(T)/MM		5.42	2.02	9.17
75	-1.02	DFT/MM	-16.62	6.79	2.05	
		DFT/COSMO		10.59	2.10	
		CCSD(T)/MM		9.12	2.12	12.25
85	-0.59	DFT/MM	-6.71	11.07	2.16	
		DFT/COSMO		14.73	2.19	
		CCSD(T)/MM		13.08	2.24	
95	-0.16	DFT/MM	3.21	16.01	2.30	
		DFT/COSMO		20.02	2.40	
		CCSD(T)/MM		17.85	2.38	
105	0.28	DFT/MM	13.36	21.68	2.47	
		DFT/COSMO		25.76	2.44	
		CCSD(T)/MM		22.78	2.64	
115	0.71	DFT/MM	23.27	28.04	2.74	
		DFT/COSMO		32.43	2.65	
		CCSD(T)/MM		25.22	2.90	
120	0.93	DFT/MM	28.35	31.72	2.99	
		DFT/COSMO		35.16	2.79	
		CCSD(T)/MM				

mol error). The nature of this agreement cannot be certain as the range of low reduction potentials corresponds to the stretched C–Cl bond that is outside the equilibrium region where COSMO parameters are expected to be most accurate. Overall, our results suggest that in aqueous solutions the degradation of CCl₄ over a wide range of reducing agents involves concerted electron transfer and bond-breaking mechanism.

IV. Conclusion

Free energy activation barriers for the reductive dechlorination (dissociative electron attachment) of carbon tetrachloride CCl₄ in aqueous phase were determined from the dissociation profiles of CCl₄ and •CCl₄⁻ using QM/MM methodology. The accuracy of the activation barriers was found to be sensitive to the level of QM description, requiring high-level CCSD(T) to get reliable results. The advantage of the explicit solvent description is demonstrated by comparing to continuum solvent (COSMO) calculations, which show significant deviations (~6 kcal/mol errors in activation barriers) in the region of long C–Cl bonds. This problem is likely due to the use the same set of COSMO parameters for both equilibrium and stretched bond regions.

In the range of reduction potentials from -2.32 to 0.93 V, CCSD(T)/MM calculations predict activation barriers from 0.7 to 35.2 kcal/mol. These results show good agreement with the experimental data for oxide-free iron surfaces (-0.6 to -1.2V reduction potentials), indicating that the measured activation barriers are consistent with concerted electron-transfer bond breaking mechanism of CCl₄ dechlorination for these reducing agents.

The results of this study illustrate that accurate ab initio electronic structure methods combined with explicit classical solvent description provide a useful and reliable tool to study ET-assisted degradation of chlorinated organic compounds in solution and potentially other reactions processes relevant to

environmental chemistry. The computational methodology illustrated in this work may also provide a useful framework for free energy calculations in conjunction with hybrid discrete/continuum⁶⁶ and other⁶⁷ approaches.

Acknowledgment. This research was supported by DOE ASCR Multiscale Mathematics program, DOE BES Geosciences program, DOE BES Nanoscale Science, Engineering, and Technology program, and ONR. The Pacific Northwest National Laboratory is operated by Battelle Memorial Institute. Some of the calculations were performed on the MPP2 computing system at the Molecular Science Computing Facility in the William R. Wiley Environmental Molecular Sciences Laboratory (EMSL) at PNNL. EMSL operations are supported by the DOE's Office of Biological and Environmental Research. We also wish to thank the Scientific Computing Staff, Office of Energy Research, and the U.S. Department of Energy for a grant of computer time at the National Energy Research Scientific Computing Center (Berkeley, CA).

References and Notes

- (1) Dilling, W. L.; Tefertiller, N. B.; Kallos, G. J. *Environ. Sci. Technol.* **1975**, *9*, 833.
- (2) Kriegman-King, M. R.; Renhard, M. *Environ. Sci. Technol.* **1992**, *26*, 2198.
- (3) Weckhuysen, B. M.; Mestl, G.; Rosynek, M. P.; Krawietz, T. R.; Haw, J. F.; Lunsford, J. H. *J. Phys. Chem. B* **1998**, *102*, 3773.
- (4) Amonette, J. E.; Workman, D. J.; Kenedy, D. W.; Fruchter, J. S.; Gorby, Y. A. *Environ. Sci. Technol.* **2000**, *34*, 4606.
- (5) Tsuchida, T.; Yasuyama, T.; Higuchi, K.; Watanabe, A.; Urakami, T.; Akaike, T.; Sato, K.; Maedah. *J. Gastroenterol. Hepatol.* **1993**, *8*, 342.
- (6) Curtiss, G. P.; Reinhard, M. *Environ. Sci. Technol.* **1994**, *28*, 2393.
- (7) Perlinger, J. A.; Angst, W.; Schwarzenbach, R. P. *Environ. Sci. Technol.* **1996**, *30*, 3408.
- (8) Perlinger, J. A.; Buschmann, J.; Schwarzenbach, R. P. *Environ. Sci. Technol.* **1998**, *32*, 2431.
- (9) Maymo-Gatell, X.; Chien, Y.; Gossett, J. M.; Zinder, S. H. *Science* **1997**, *267*, 1568.

- (10) Holliger, C.; Wohlfarth, G.; Diekert, G. *FEMS Microbiol. Rev.* **1998**, *22*, 383.
- (11) Schwarzenbach, R. P.; Gschwend, P. M.; Imboden, D. M. *Environmental Organic Chemistry*; John Wiley & Sons, Inc.: New York, 1993.
- (12) Costentin, C.; Robert, M.; Saveant, J. M. *J. Am. Chem. Soc.* **2003**, *125*, 10729.
- (13) Paulino, J. A.; Squires, R. R. *J. Am. Chem. Soc.* **1991**, *113*, 5573.
- (14) Martin, J. D. D.; Hepburn, J. W. *J. Chem. Phys.* **1998**, *109*, 8139.
- (15) Bylaska, E. J.; Dixon, D. A.; Felmy, A. R.; Tratnyek, P. G. *J. Phys. Chem. A* **2002**, *106*, 11581.
- (16) Tratnyek, P. G.; Weber, E. J.; Schwarzenbach, R. P. *Environ. Toxicol. Chem.* **2003**, *22*, 1733.
- (17) Scherer, M. M.; Balko, B. A.; Gallagher, D. A.; Tratnyek, P. G. *Environ. Sci. Technol.* **1998**, *32*, 3026.
- (18) Bylaska, E. J.; Dixon, D. A.; Felmy, A. R. *J. Phys. Chem. A* **2000**, *104*, 610.
- (19) Bylaska, E. J.; Dixon, D. A.; Felmy, A. R.; Apra, E.; Windus, T. L.; Zhan, C.-G.; Tratnyek, P. G. *J. Phys. Chem. A* **2004**, *108*, 610.
- (20) Bylaska, E. J.; Dupuis, M.; Tratnyek, P. G. *J. Phys. Chem. A* **2005**, *109*, 5905.
- (21) Arnold, W. A.; Wignet, P.; Cramer, C. J. *Environ. Sci. Technol.* **2002**, *36*, 3536.
- (22) Nonnenberg, C.; van der Donk, W. A.; Zipzse, H. *Phys. Rev. A* **2002**, *106*, 8708.
- (23) Patterson, E. V.; Cramer, C. J.; Truhlar, D. G. *J. Am. Chem. Soc.* **2001**, *123*, 2025.
- (24) Borisov, Y. A.; Arcia, E. E.; Mielke, S. L.; Garrett, B. C.; Dunning, J. T. H. *J. Phys. Chem. A* **2001**, *105*, 7724.
- (25) Winget, P.; Cramer, C.; Truhlar, D. *Theor. Chem. Acc.* **2004**, *112*, 217.
- (26) Perlinger, J. A.; Venkatapathy, R.; Harrison, J. F. *J. Phys. Chem. A* **2000**, *104*, 2752.
- (27) Feller, D.; Peterson, K.; de Jong, W.; Dixon, D. *J. Chem. Phys.* **2003**, *118*, 3510.
- (28) Soriano, A.; Silla, E.; Tunon, I. *J. Chem. Phys.* **2002**, *116*, 6102.
- (29) Bertran, J.; Gallardo, I.; Moreno, M.; Saveant, J. M. *J. Am. Chem. Soc.* **1992**, *114*, 9576.
- (30) Tada, T.; Yoshimura, R. *J. Am. Chem. Soc.* **1992**, *114*, 1593.
- (31) Pause, L.; Robert, M.; Saveant, J. *J. Am. Chem. Soc.* **2000**, *122*, 9829.
- (32) Sun, H.; Bozzelli, J. W. *J. Phys. Chem. A* **2001**, *105*, 4504.
- (33) Booty, M. R.; Bozzelli, J. W.; Ho, W. P.; Magee, R. S. *Environ. Sci. Technol.* **1995**, *29*, 3059.
- (34) Chen, C.; Wong, D.; Bozzelli, J. *J. Phys. Chem. A* **1998**, *102*, 4551.
- (35) Sun, H.; Bozzelli, J. *J. Phys. Chem. A* **2003**, *107*, 1018.
- (36) Zhang, N.; Blowers, P.; Farrell, J. *Environ. Sci. Technol.* **2005**, *39*, 612.
- (37) Bylaska, E. J. *Theor. Chem. Acc.* **2006**, *116*, 281.
- (38) Klamt, A.; Schuurmann, G. *J. Chem. Soc., Perkin Trans. 2* **1993**, *1993*, 799.
- (39) Cossi, M.; Barone, V.; Cammi, R.; Tomasi, J. *Chem. Phys. Lett.* **1996**, *255*, 327.
- (40) Friesner, R. A.; Guallar, V. *Annu. Rev. Phys. Chem.* **2005**, *56*, 389.
- (41) Gao, J. L.; Truhlar, D. G. *Annu. Rev. Phys. Chem.* **2002**, *53*, 467.
- (42) Valiev, M.; Garrett, B. C.; Tsai, M.-K.; Kowalski, K.; Kathmann, S. M.; Schenter, G. K.; Dupuis, M. *J. Chem. Phys.* **2007**, *127*, 51102.
- (43) Bartlett, R. J., and J. F. Stanton. In *Reviews of Computational Chemistry*; Lipkowitz, K. B., Boyd, D. B., Ed.; VCH Publishers: New York, 1995; Chapter 2, pp 65–169.
- (44) Bartlett, R. J.; Musial, M. *Rev. Mod. Phys.* **2007**, *79*, 291.
- (45) Saveant, J. M. *J. Am. Chem. Soc.* **1987**, *109*, 6788.
- (46) Saveant, J. M. *Acc. Chem. Res.* **1993**, *26*, 455.
- (47) Becke, A. D. *J. Chem. Phys.* **1993**, *98*, 5648.
- (48) Lee, C.; Yang, W.; Parr, R. G. *Phys. Rev. B* **1988**, *37*, 785.
- (49) Francl, M. M.; Petro, W. J.; Hehre, W. J.; Binkley, J. S.; Gordon, M. S.; DeFrees, D. J.; Pople, J. A. *J. Chem. Phys.* **1982**, *77*, 3654.
- (50) Dunning, T. H. *J. Chem. Phys.* **1989**, *90*, 1007.
- (51) Apra, E.; Windus, T. L.; Straatsma, T. P.; Bylaska, E. J.; de Jong, W.; Hirata, S.; Valiev, M.; Hackler, M. T.; Pollack, L.; Kowalski, K.; Harrison, R. J.; Dupuis, M.; Smith, D. M. A.; Nieplocha, J.; Tipparaju, V.; Krishnan, M.; Brown, E.; Cisneros, G.; Fann, G. I.; Fruchtl, H.; Garza, J.; Hirao, K.; Kendall, R.; Nichols, J. A.; Tsemekhman, K.; Wolinski, K.; Ansell, J.; Bernholdt, D.; Borowski, P.; Clark, T.; Clerc, D.; Dachsel, H.; Deegan, M.; Dyall, K.; Elwood, D.; Glendening, E.; Gutowski, M.; Hess, A.; Jaffe, J.; Johnson, B.; Ju, J.; R. Kobayashi, R.; Kutteh, R.; Lin, Z.; Littlefield, R.; Long, X.; Meng, B.; Nakajima, T.; Niu, S.; Rosing, M.; Sandrone, G.; Stave, M.; Taylor, H.; Thomas, G.; van Lenthe, J.; Wong, A.; Zhang, Z. *NWChem, A Computational Chemistry Package for Parallel Computers*, 4.7 ed.; Pacific Northwest National Laboratory: Richland, WA, 2005.
- (52) Garrett, B. C.; Schenter, G. K. *Int. Rev. Phys. Chem.* **1994**, *13*, 263.
- (53) Berendsen, H. J. C.; Grigera, J. R.; Straatsma, T. P. *J. Phys. Chem.* **1987**, *91*, 6269.
- (54) Fox, T.; Kollman, P. A. *J. Phys. Chem. B* **1998**, *102*, 8070.
- (55) Zhang, Y. K.; Liu, H. Y.; Yang, W. T. *J. Chem. Phys.* **2000**, *112*, 3483.
- (56) Zwanzig, R. W. *J. Chem. Phys.* **1954**, *22*, 1420.
- (57) Stefanovich, E. V.; Truong, T. N. *Chem. Phys. Lett.* **1995**, *244*, 65.
- (58) Ebersson, L. *Acta Chem. Scand.* **1999**, *53*, 751.
- (59) Piecuch, P. *J. Mol. Struct.* **1997**, *436–437*, 503.
- (60) Roszak, S.; Koski, W.; Kaufman, J.; Balasubramanian, K. *J. Chem. Phys.* **1997**, *106*, 7709.
- (61) Spence, D.; Schulz, G. J. *J. Chem. Phys.* **1973**, *58*, 1800.
- (62) Tissandier, M. D.; Cowen, K. A.; Feng, W. Y.; Gundlach, E.; Cohen, M. H.; Earhart, A. D.; Coe, J. V.; Tuttle, T. R., Jr. *J. Phys. Chem. A* **1998**, *102*, 7787.
- (63) Wagman, D. D. *J. Phys. Chem. Ref. Data* **1982**, *11*, Suppl. 2.
- (64) Chase, J.; M. W. *Phys. Chem. Ref. Data* **1998**, *9*, 1.
- (65) Li, T.; Farrell, J. *Environ. Sci. Technol.* **2001**, *35*, 3560.
- (66) Brancato, G.; Barone, V.; Rega, N. *Theor. Chem. Acc.* **2007**, *117*, 1001.
- (67) Hirata, S.; Valiev, M.; Dupuis, M.; Xantheas, S. S.; Sugiki, S.; Sekino, H. *Mol. Phys.* **2005**, *103*, 2255.